CSCE Annual Conference

Growing with youth – Croître avec les jeunes

Laval (Greater Montreal)

June 12 - 15, 2019

SEISMIC PERFORMANCE ANALYSIS OF HIGH-RISE RC SHEAR WALLS REINFORCED WITH SUPERELASTIC SHAPE MEMORY ALLOYS

Maciel, M.[1,3], Cortés-Puentes, W. L.[2] and Palermo, D.[1]
[1] York University, Canada
[2] National Research Council Canada
[3] mmaciel1@yorku.ca

Abstract: The seismic performance of hybrid Shape Memory Alloy (SMA)-steel concrete shear walls containing Nickel-Titanium (Ni-Ti) superelastic SMA as alternative reinforcement in the plastic hinge zone is investigated. This wall system permits self-centering with high levels of energy dissipation and significant reduction of permanent deformations. A ductile type of Reinforced Concrete (RC) shear wall was investigated for a prototype 10-storey office building in the seismic design scenario of western Canada. The wall was designed according to the current Canadian design standards as conventional deformed steel-reinforced concrete shear wall. The resulting cross-section was used to define the geometry and reinforcement layout of equivalent hybrid SMA-steel RC wall. Full-scale 2-D Finite Element (FE) models of the walls were developed and subjected to nonlinear reverse cyclic analyses. Similarities in cross-section permitted a reliable comparison and assessment of the post-loading condition, including displacement capacity and drift, damage, residual displacement, and energy dissipation. The observed response of the hybrid SMA-steel wall, when compared to that of the steel-reinforced wall, indicated similar lateral capacity, slightly lower energy dissipation, and superior restoring capacity. In general, the introduction of Ni-Ti bars in the plastic hinge region of shear walls showed potential to optimize the seismic performance of reinforced concrete buildings, controlling residual deformations and thereby reducing damage to structural elements.

1 INTRODUCTION

Seismic design standards around the world are primarily developed to ensure life safety of the occupants of buildings during major seismic events. In reinforced concrete structures, design provisions are developed to permit yielding of reinforcing steel bars, which works as a mechanism to dissipate the energy of large earthquakes. Due to its post-yield plastic properties, reinforcing steel results in permanent deformations. The aftermath of strong ground motions will therefore involve substantial damage to non-structural and structural components, leading to significant economic losses due to repair costs and inactivity of the building for a long period of time. Extent of damage can even render repair prohibitive and, very often, impose demolition. In order to mitigate these consequences, there has been a growing trend among the engineering community towards performance-based design and the development of high-performance structural systems with enhanced deformation capacity and ductility, higher damage tolerance, and recoverable deformations (Alam et al. 2008). In this scenario, novel lateral seismic-force-resisting systems with inherent self-centering capacity have been investigated. One way of achieving such desirable behaviour is to incorporate smart materials such as Shape Memory Alloys to conventional structural systems. SMAs are metallic alloys with the ability to sustain large deformation and to recover to a predetermined shape when heated (shape memory feature) or when loading is removed (superelastic feature). SMAs can absorb and dissipate energy by undergoing a reversible hysteretic shape change when subjected to cyclic loading.

Nickel-Titanium (Ni-Ti) alloys are of particular interest for seismic engineering applications due to characteristics such as large superelastic strain recovery, high energy dissipation, and excellent low-cycle and high-cycle fatigue properties (Tarzav and Saiidi 2015). Figure 1 illustrates the typical stress-strain response of superelastic Ni-Ti SMA. The response is characterized by an upper (UPS) and a lower (LPS) plateau stresses, initial elastic modulus (E_i), residual (El_r) and ultimate (El_u) elongations, and equivalent viscous damping (ξ_{eq} – based on the area inside the hysteretic loop) (Cortés-Puentes and Palermo 2015). The strain of 6% in Figure 1 represents the recoverable strain of Ni-Ti, and the strain of 3% corresponds to the UPS. Different combinations of temperature and stress induce reverse and forward transformations from the two phases that constitute SMAs, the Austenite and Martensite phases. Superelastic behaviour of Ni-Ti alloys correspond to the Austenite phase, which is the high temperature phase of SMAs, and follow a linear elastic response with E_i until reaching the critical stress that corresponds to the start of the Martensite variant reorientation, which is the low temperature phase of SMA. Beyond the onset of reorientation, the modulus of elasticity drops to 10-15% of E_i. For strains greater than the recoverable strain, the material becomes stiffer and the modulus of elasticity reaches 50-60% of E_i (Alam et al. 2007). Permanent deformations accumulate upon unloading at this stage and beyond, which can be recovered through heating (shape memory effect). It is important to note that yielding, as it implies permanent deformation, is not experienced by superelastic SMAs. The stress-strain response exhibits a substantial change in stiffness similar to yielding of steel. The change in stiffness, however, is due to phase transformation rather than yielding and does not incur in permanent deformation (Tarzav and Saiidi 2015).

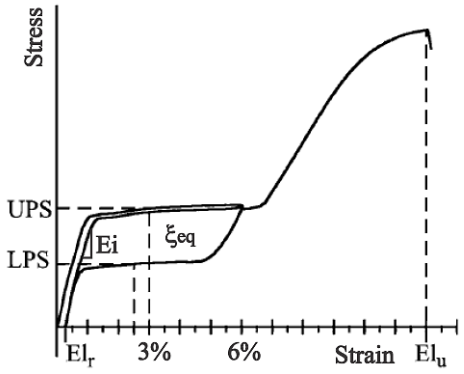

Figure 1: Typical stress-strain response of Ni-Ti SMA (Cortés-Puentes and Palermo 2015)

The possibilities of implementing superelastic SMA-based systems in structures for seismic applications are various, including bracing, bolted connections, restrainers, and prestressing strands (Alam et al. 2007), as well as the use in retrofitting systems as dampers, isolators, and post-tensioning tendons. The specific application of SMA as alternative reinforcement is still in its infancy. Several researchers have been successful in demonstrating the superior seismic response, with respect to self-centering, of concrete elements reinforced with SMA bars, such as moment-resisting frames (Youssef and Elfeki 2010), beam-column joints (Alam et al. 2008; Nehdi et al. 2011), columns (Alam et al. 2008; Cruz-Noguez and Saiidi 2013; Tarzav and Saiidi 2015) and beams (Elbahy et al. 2009; Abdulridha et al. 2013). The investigation of SMA as reinforcement in RC shear walls is, however, still limited. As of today, studies have employed numerical analysis to investigate optimal locations for SMA bars in moderate and squat RC shear walls (Abraik and Youssef 2015; Abraik and Youssef 2016) and in coupled shear walls (Ghassemieh et al. 2017). The vulnerability to seismic damage of tall concrete shear walls reinforced with SMA within plastic hinge regions has been assessed with the use of fiber models and fragility curves (Abraik and Youssef 2018). The performance of hybrid shear walls with SMA has been evaluated and compared to other innovative self-centering wall systems (Kian and Cruz-Noguez 2018). In addition, experimental testing and numerical modelling have been used to evaluate the behaviour of slender hybrid RC walls containing SMA prior to and after repair (Cortés-Puentes et al. 2018). Results from these studies demonstrated excellent self-centering and restoring capacity of the hybrid SMA-steel RC walls, negligible residual deformations, localized damage in the plastic hinge region, stable hysteretic response with substantial energy dissipation, and acceptable serviceability performance requiring minimum repair after severe cyclic loading. Furthermore, experimental tests and complementary numerical studies have demonstrated that hybrid

SMA-steel RC shear walls can recover large inelastic displacements in spite of the presence of steel reinforcement in the web portion of the wall (Abdulridha and Palermo 2017). Numerical studies of the effects of axial load in the restoring capacity of hybrid SMA-steel walls have also demonstrated the energy dissipation capabilities of SMA-reinforced concrete shear walls and the levels of axial load after which SMA does not offer improvements in response (Maciel et al. 2016). Given the improvements in behavioural response, hybrid SMA-reinforced concrete walls have become an alternative to traditional structural systems in earthquake-prone buildings, specifically if direct and indirect costs related to seismic performance, including repair and downtime, are considered. However, complete understanding of the behaviour of SMA-reinforced concrete elements, specifically in self-centering shear walls, still requires extended research in order to develop a robust database that can validate analytical models and culminate in the development of design provisions custom-made to permit the most effective use of this innovative material.

1.1 Research significance

The hybrid SMA-steel RC shear wall investigated in this study aims to achieve optimal seismic performance with high self-centering capacity, controlled damage, reduced residual deformations, and significant energy dissipation. When applied to building structures, this behaviour will potentially reduce and simplify post-earthquake repairs, rendering buildings functional more readily and drastically minimize economical losses after seismic hazards. In order to implement hybrid SMA-steel RC walls into structures, a comprehensive understanding of the seismic response of the structure as a whole is paramount. Most of the available studies have focused on the analysis of single-storey walls, which might hinder a complete evaluation of the implications associated with the use of SMA as reinforcement in shear walls of multistorey dimensions. To address this issue, this paper investigates the response of full-scale, high-rise shear walls by conducting non-linear analyses with the finite element program VecTor2 (Vecchio et al. 2013). This paper presents results of preliminary reverse cyclic analysis on ductile walls designed for western Canada.

2 DESIGN OF THE SHEAR WALLS

Figure 2 illustrates the prototype building used in the study. The building has a typical floor plan of 42 m × 36 m, a 3.5 m-high first storey, and nine 3.0 m-high storeys from level 2 to 10. Lateral resistance to earthquakes is provided by four RC shear walls in each orthogonal direction. The floor plan and arrangement of the walls led to larger torsional effects in one principal direction. Thus, a typical shear wall was designed for the critical direction and adopted for the other walls.

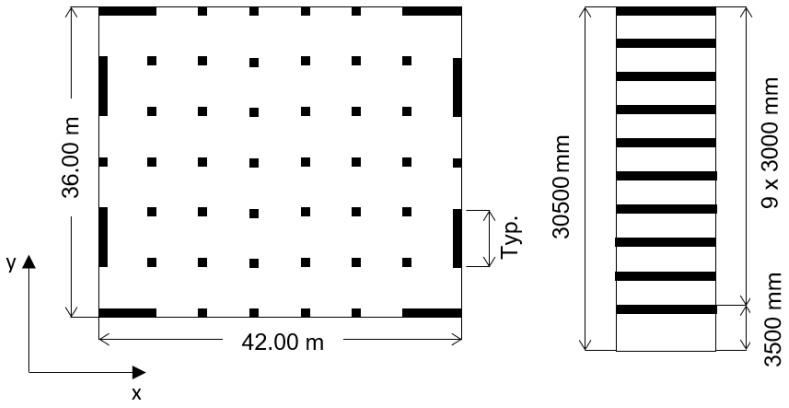

Figure 2: Plan view and wall elevation of building under study

A conventional, ductile steel-reinforced shear wall (wall DSRW) was designed according to the seismic detailing provisions prescribed by the 2015 National Building Code of Canada (NRC 2015), for the design location of Vancouver – BC, and the Canadian Standards Association Standard A23.3-14 Design of Concrete Structures (CSA 2014). The shear wall was designed as the seismic-force-resisting system of the building. Columns were considered part of the gravity-load-carrying system, and not to experience inelastic

response when subjected to the seismic displacements. Flat slabs were considered with a thickness of 225 mm. The building is assumed to be on firm ground, corresponding to Soil Site Class C in the NBCC-2015 (NRC 2015). To verify the fundamental period of the structure and carry out the design process, a 3-D model of the building was developed in a structural analysis program. Dynamic modal response spectrum analyses were conducted to determine the seismic force demands and displacements of the structure.

Details of wall DSRW are illustrated in Figure 3 (a) and (c). The minimum thickness required for wall DSRW was 350 mm. To develop the desired rotational capacity of wall DSRW, concentrated reinforcement was provided along a distance equal to 500 mm from the edges and tied with confinement reinforcement. In each of these boundary regions, sixteen-25M bars (25.2 mm diameter) were specified as longitudinal reinforcement and were tied with three sets of 10M (11.3 mm diameter) closed stirrups spaced vertically at 140 mm. The ratio of distributed horizontal reinforcement was selected as the minimum required of 0.25%. Vertical distributed reinforcement was provided with 15M bars (16 mm diameter) spaced at 230 mm. All distributed reinforcement was arranged in two layers. Although the code limits would permit a reduction in thickness and reinforcement ratio above the plastic hinge region of the wall, the cross-section at the base of the wall was extended to the other storey levels. Thus, irregularities in stiffness were prevented, simplifying the understanding of the link between the response of the wall and the presence of SMA. The plastic hinge was expected to form at the base of the wall and to extend over a height of 6.05 m, calculated according to the NBCC-2015 (NRC 2015).

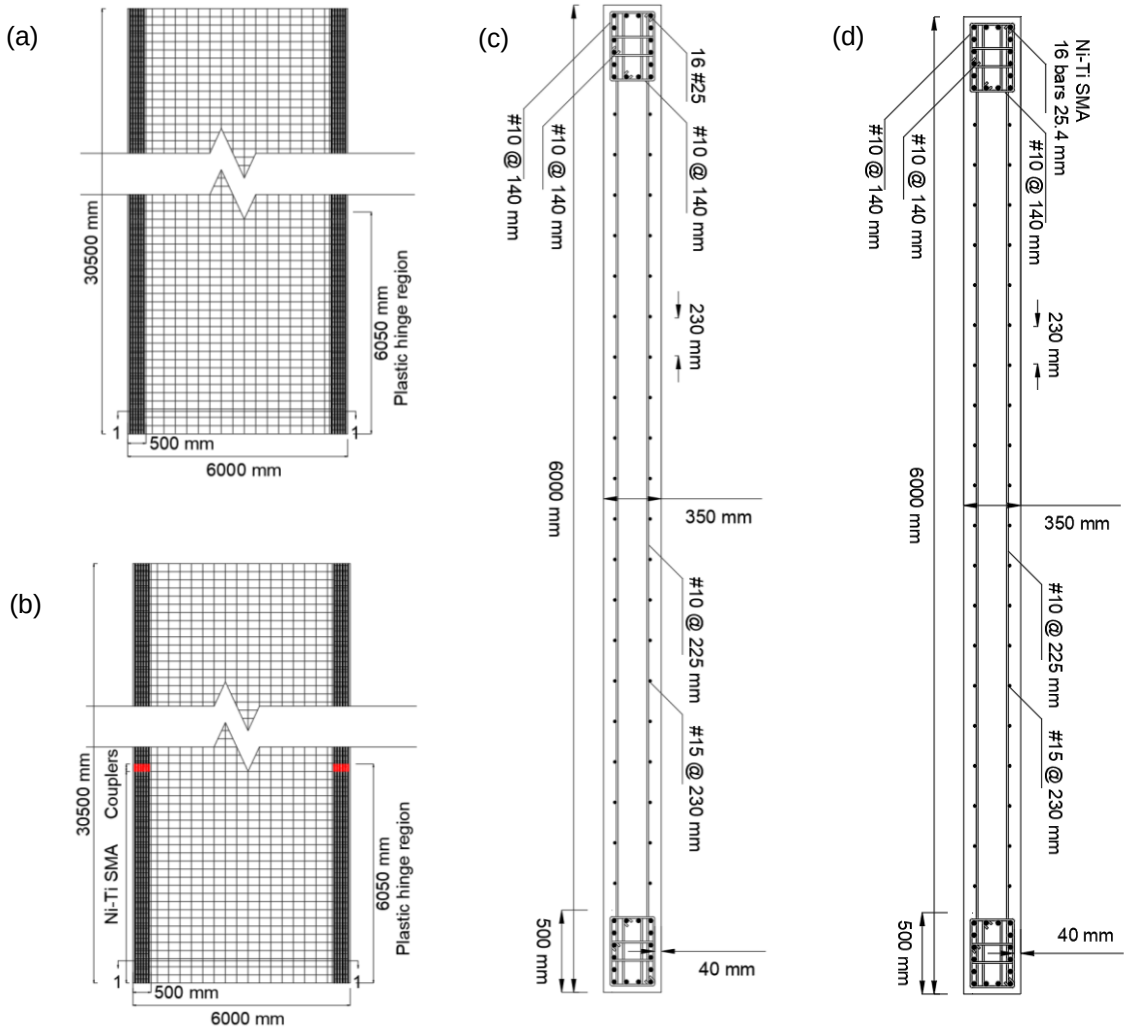

Figure 3: Details of walls: (a) elevation of wall DSRW, (b) elevation of wall DHW, (c) cross-section of wall DSRW, and (d) cross-section of wall DHW

Details of wall DHW are illustrated in Figure 3 (b) and (d). Wall DHW was developed based on the design of the conventional steel-reinforced wall, given the lack of explicit provisions for seismic design of SMA-reinforced concrete members. Comparable dimensions and reinforcement details were adopted, except for the deformed-steel longitudinal reinforcement in the plastic hinge zone at the boundaries of the wall, which was replaced with Ni-Ti superelastic SMA bars with diameter similar to the longitudinal reinforcement in wall DSRW. SMA bars are connected to the steel bars above the plastic hinge region through mechanical couplers modelled as stiff. The remaining reinforcement details were consistent with that of the steel-reinforced wall. Mechanical properties adopted in design and modelling of the shear walls are listed in Table 1.

Table 1: Mechanical properties of concrete and reinforcement materials

Material property	Value
Compressive concrete strength (f'_c)	30 MPa
Yielding strength of steel (f_y)	400 MPa
Ultimate strength of steel (f_u)	600 MPa
Modulus of elasticity of SMA (E_s)	38000 MPa
Strain hardening strain of SMA (ε_{sh})	6%
Ultimate strain of SMA (ε_{su})	20%
Yielding strength of SMA (f_y)	400 MPa
Ultimate strength of SMA (f_u)	1000 MPa

3 NUMERICAL ANALYSIS

Nonlinear reverse cyclic analyses were performed with FE program VecTor2 (Vecchio et al. 2013) to determine the capacity, failure mechanism, residual drift, recentering, and energy dissipation of the walls. VecTor2 considers the combined effects of shear and flexure to predict the seismic response and damage of reinforced concrete elements. VecTor2 program has been previously used to accurately predict the response of a slender RC shear wall reinforced with Ni-Ti SMA bars in the plastic hinge region within the boundary zones (Abdulridha and Palermo 2017). Furthermore, the program has been used to appropriately predict the shear force distribution envelope of RC shear walls under seismic events when test results are not available (Luu et al. 2013). The program has been further acknowledged to effectively predict the inelastic monotonic and cyclic behaviour of ductile shear walls (Ghorbani-Renani et al. 2009).

Figure 4 illustrates the finite element models of walls DSRW and DHW. Three concrete regions (1, 2 and 3) were defined and modelled with plane stress rectangular elements. The first region included a rigid base foundation (800 mm deep × 1500 mm wide) and a top slab (225 mm thick × 1500 mm wide), where all reinforcement was considered smeared in the concrete elements. The width of the top slab corresponds to the width tributary to the walls. The second region defined the web zone of the walls, with transverse shear reinforcement and longitudinal reinforcement smeared in the concrete elements. The third region corresponded to the boundary zones of the walls, where truss elements were adopted to discretize the SMA and steel longitudinal reinforcement, whereas the transverse shear reinforcement and confinement reinforcement were smeared. The mesh consisted of approximately 200 mm × 200 mm elements, with the exception of the boundary zones, where the element dimension was 74 mm × 202 mm due to constraints imposed by the truss bar elements. The connection between SMA and steel bars was modelled as a stiff steel coupler with diameter greater than that of the bars. Steel elements were defined as fully bonded with the surrounding concrete, whereas SMA bars were modelled as embedded smooth bars interacting with concrete through link elements. The Eligehausen model (Eligehausen et al. 1983) was used to define the stress-slip relationship of the link elements. Other material models adopted in the analysis corresponded to the default models of the program. Detailed description of these models can be found elsewhere (Vecchio et al. 2013). The walls had an axial load ratio ($P/A_g f'_c$) of 6.90% applied at the top slab, which corresponded to the gravity loads acting on the building and within the tributary area of the walls, and were subjected to reverse cyclic analysis at increments of the yield displacement.

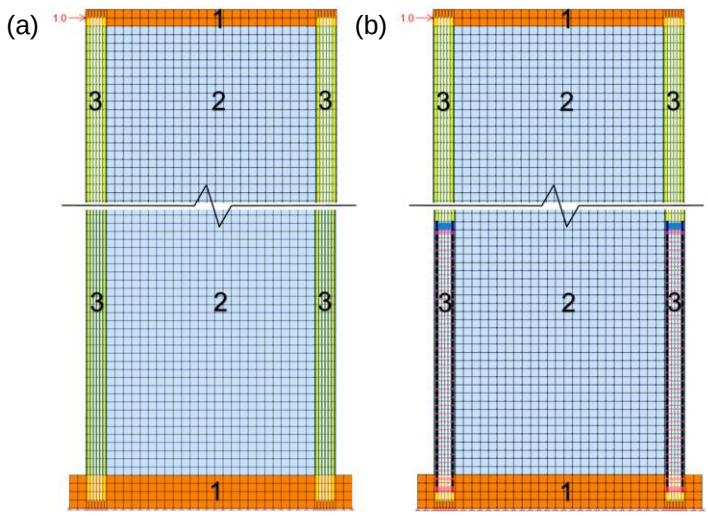

Figure 4: FE models of the walls: (a) DSRW and (b) DHW

4 ANALYSIS RESULTS AND DISCUSSION

4.1 Load-displacement hysteretic response

The hysteretic response of the walls resulting from the analysis is shown in Figure 5. In general, the hysteretic response of the walls was stable and symmetric, without signs of brittle failure. Walls DSRW and DHW sustained lateral peak strengths (F_{max}) of 1413.5 KN and 1342.8 KN, respectively. The strength of wall DHW was only 5% lower than wall DSRW. The calculated effective stiffness (k_{eff}) was 6.5 KN/mm for DSRW and 2.8 KN/mm for DHW. k_{eff} corresponded to the slope of the loading branch going through the yield point (pseudo-yield point in DHW), which was determined by the reduced stiffness equivalent elasto-plastic yield method (Park 1988) for both positive and negative directions of cyclic response. The lower k_{eff} of wall DHW, 43% of k_{eff} of DSRW, was expected given the lower modulus of elasticity of Ni-Ti SMA bars. This reduction in stiffness, however, does not infer an inferior seismic response. A lower stiffness elongates the fundamental period of the structure, which, in turn, would result in lower seismic forces if the walls were to be redesigned. Walls DSRW and DHW experienced displacement ductilities (μ) of 7.5 and 2.7, respectively. These ductilities correspond to ultimate displacements (δ_u) of 1366.8 mm and 1129.2 mm, respectively. It was observed that rupture of the reinforcing steel in the web zone reduced the ductility of the SMA-reinforced wall. The lower displacement ductility of wall DHW can also be attributed to the much higher pseudo-yield displacement (onset of reorientation) of this wall. The displacement ductility was determined as the ratio of the ultimate displacement (δ_u) to the yield displacement (δ_y), both for positive and negative displacements. The ultimate displacement was determined as the displacement corresponding to a drop of 20% in the lateral strength of the wall, or 0.8 F_{max}. Note; however, that a more appropriate comparison between the walls is the drift capacity.

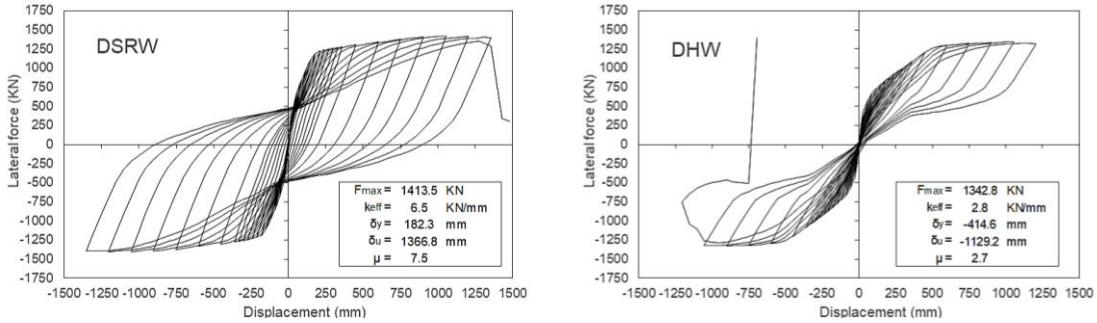

Figure 5: Lateral load-displacement hysteretic response of walls

4.2 Failure mechanism and cracking pattern

Figure 6 provides the displaced shape of the lower portion of the walls combined with the predicted crack pattern. Figure 6 (a) and (c) illustrate the state of the walls at the peak of the cycle corresponding to 2.5% drift. Figure 6 (b) and (d) display the walls at the zero load following the 2.5% drift. Failure of the walls was evaluated based on the stresses and strains in the SMA and steel reinforcements and concrete. The longitudinal reinforcement in the web and boundary zones yielded at early stages of loading in both walls. In wall DSRW, a local shear failure (large shear distortion of the concrete elements) was observed at the interface between the boundary and web regions, which is attributed to the large difference in reinforcement ratio between the two regions. Global failure occurred when the concentrated longitudinal steel bars in the boundary zone ruptured concurrently with crushing of the concrete at the base of the wall during the last cycle. This was followed by shear sliding and horizontal cracking along the base of the wall.

In wall DHW, the presence of SMA bars shifted the critical section slightly above the base of the wall. At the critical section, large horizontal cracking surfaced, and fracture of the longitudinal steel bars in the web zone was captured. The lateral capacity of wall DHW was reduced by failure of the steel reinforcement in the web zone. Further analyses, varying the reinforcement ratio in the web zone, demonstrated the strong influence of the web reinforcement on the response of wall DHW. The smooth surface of SMA bars leads to concentration of damage at localized cracks in the concrete, in contrast with the more distributed cracks that are generated due to the stronger bond of deformed steel to concrete. The SMA bars remained within the superelastic range during the entire analysis, not fracture or buckling, but experiencing pseudo-yielding at around 0.5% drift.

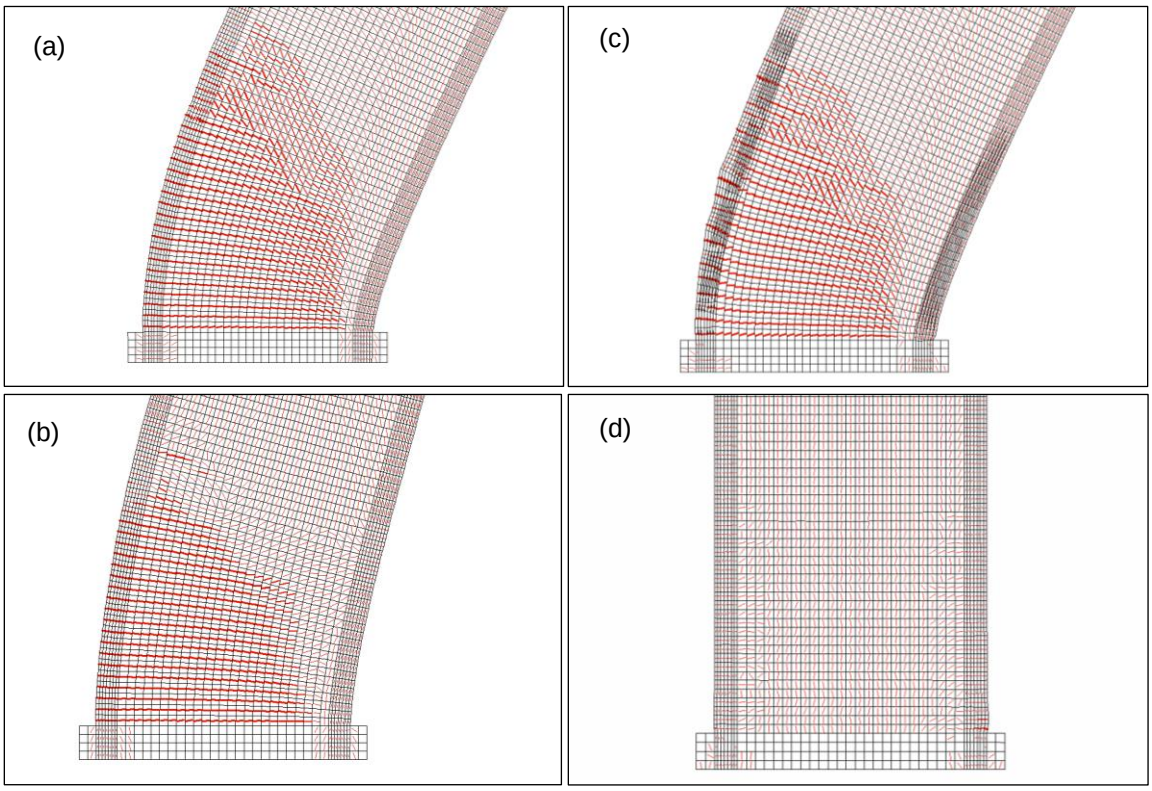

Figure 6: Displaced shape and crack pattern of: wall DSRW (a) at peak drift of 2.5% and (b) at zero load, and wall DHW (c) at peak drift of 2.5% and (d) at zero load

4.3 Energy dissipation

Figure 7 (a) provides a hysteresis loop of the walls at the drift ratio of 2.5%. The response of wall DHW exhibits a more pronounced pinching than wall DSRW. Pinching in wall DHW is primarily due to the superelastic response of the SMA bars. Conversely, wider hysteretic loops in wall DSRW are the result of yielding of the reinforcing steel. The energy dissipated by the walls during each cycle was calculated based on the area of the force-displacement loop. The cumulative dissipated energy versus drift for the walls is shown in Figure 7 (b). The energy dissipation capacity of wall DSRW showed a more pronounced increase than wall DHW. There was a noticeable increase in the energy dissipated by the steel-reinforced wall at higher drifts. At a drift of 2.5%, wall DHW dissipated 1747 KNm of energy, while wall DSRW dissipated 4524 KNm. In total, the energy dissipated by wall DHW was equal to 38% of the energy dissipated by wall DSRW. The lower energy dissipation capacity in wall DHW relates to the flag-shaped hysteretic behaviour with significant pinching and does not necessarily implicate in inferior seismic performance. Numerical results have demonstrated that flag-shaped hysteretic behaviour in low-strength systems provide equivalent or even improve the seismic response of the system relative to an elastic-plastic hysteretic behaviour (Christopoulos et al. 2002).

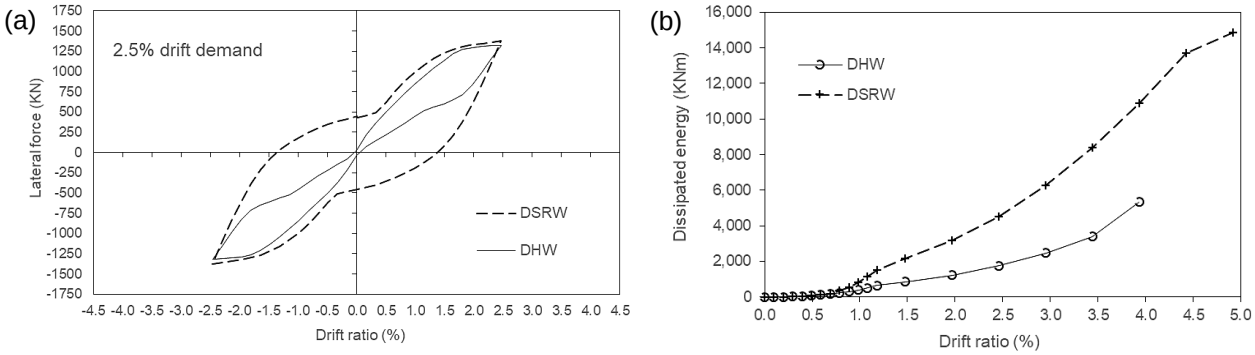

Figure 7: Energy dissipation of walls: (a) hysteretic cycle at 2.5% drift, and (b) cumulative dissipated energy

4.4 Self-centering capacity

Figure 8 (a) illustrates the lateral load versus drift envelope response of the walls. The drifts were calculated from the top displacement divided by the height of the wall, which corresponds to the point where displacements were applied in the analysis. Wall DHW sustained drifts up 4.0%, whereas maximum drift in wall DSRW was 4.5%.

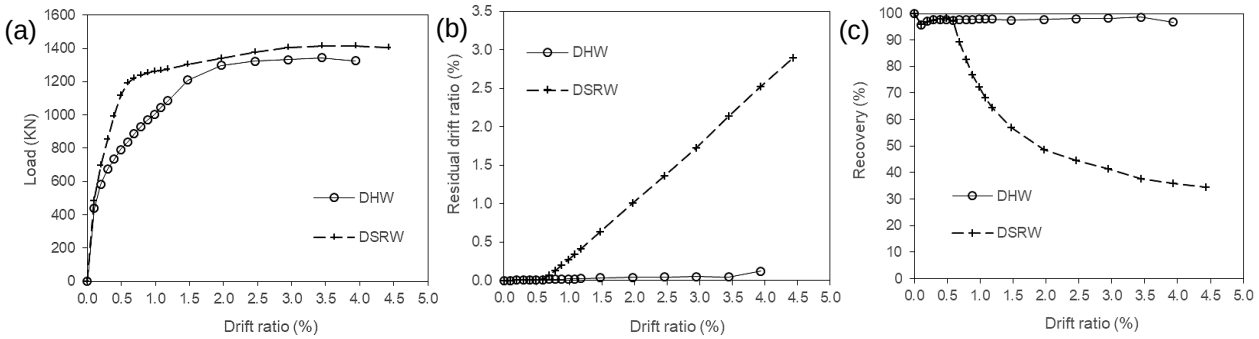

Figure 8: Self-centering capacity of the walls: (a) envelope of lateral load-drift response, (b) residual drift - peak drift response, and (c) recovery-drift response

Figure 8 (b) presents residual drift versus peak drift of the walls. The residual drift of the walls corresponded to the drift at the completion of unloading. Residual drifts in wall DSRW became evident at a drift of 0.7%

and increased almost linearly thereafter. At a peak drift of 3.0%, a residual drift of 1.73% was exhibited in wall DSRW. Wall DHW initially experienced residual drifts similar to wall DSRW. However, at a drift of 0.6%, the steel bars in the web yielded and the SMA bars became more effective at recentering the wall. Beyond 0.6% drift, wall DHW maintained smaller residual drifts for all peak drifts in comparison to wall DSRW, showing a residual drift of 0.05% at 3.0% peak drift, which represents a reduction in residual drift of 97%. Figure 8 (c) illustrates the recovery capacity of the walls. The recovery was calculated as the ratio of the difference between the peak and residual drift to the peak drift at each drift. At a drift of 2.5%, wall DHW provided a recovery capacity of 98% compared to the approximate recovery capacity of 45% of wall DSRW. Wall DHW sustained significantly smaller residual drifts than wall DSRW, demonstrating higher self-centering capacity. The self-centering effect of SMA is further confirmed by the realigned position of wall DHW upon unloading (Figure 6 (d)) compared to the significant permanent deformation of wall DSRW (Figure 6 (b)).

5 CONCLUSIONS

This study investigated the benefits of implementing hybrid SMA-steel reinforcing system in high-rise reinforced concrete shear walls by comparing the response of an alternative SMA-reinforced wall with the response of a companion conventional steel-reinforced wall. Numerical simulations using finite element modelling were performed. The following conclusions can be drawn from the study:

1- Both the SMA-reinforced and the steel-reinforced concrete walls maintained a stable response beyond the code limit for lateral top drift of 2.5%, without suffering significant loss in load carrying capacity, and ensuring a satisfactory response. The SMA-reinforced wall sustained high levels of drift without exhibiting significant permanent deformation.

2- The SMA-reinforced wall experienced less displacement ductility when compared to the steel-reinforced wall. The reduction in displacement ductility was due to rupture of the reinforcing steel in the web zone of the SMA-reinforced wall.

3- The stiffness of the SMA-reinforced wall was 57% lower than that of the steel-reinforced wall, which was attributed to the lower modulus of elasticity of Ni-Ti SMA bars compared to that of the steel bars.

4- The SMA-reinforced wall demonstrated substantially higher recovery capacity than the steel-reinforced wall. At the end of analysis, recovery of wall DHW was 97%, while the recovery of wall DSRW was 34.5%.

5- The steel-reinforced wall dissipated more energy than the SMA-reinforced wall. The lower energy dissipation capacity, however, does not necessarily imply deficient seismic performance, as flag-shaped hysteretic behaviour, such as that of SMA, can provide stable seismic responses due to the combined effect of adequate energy dissipation and significant self-centering capacity.

In brief, the proposed hybrid reinforcing system resulted in wall strengths comparable to that of steel-reinforced walls. The SMA reinforcement was effective in controlling permanent deformations and demonstrated superior self-centering capabilities with significant energy dissipation.

References

Abdulridha, A. and Palermo, D. 2017. Behaviour and modelling of hybrid SMA-steel reinforced concrete slender shear wall. *Engineering Structures*, Elsevier, **147**:77-89.

Abdulridha, A., Palermo, D., Foo, S. and Vecchio, F.J. 2013. Behavior and modeling of superelastic shape memory alloy reinforced concrete beams. *Engineering Structures*, Elsevier, **49**:893-904.

Abraik, E. and Youssef, M.A. 2015. Cyclic performance of shape memory alloy reinforced concrete walls. *Conference on Response of Structures under Extreme Loading*, East Lansing, MI, USA.

Abraik, E. and Youssef, M.A. 2016. Performance assessment of three-story shape memory alloy reinforced concrete walls. *Resilient Infrastructure*, London, **852**:1-9.

Abraik, E. and Youssef, M.A. 2018. Seismic fragility assessment of superelastic shape memory alloy reinforced concrete shear walls. *Journal of Building Engineering*, Elsevier, **19**:142-153.

Alam, M.S., Youssef, M.A. and Nehdi, M. 2008. Analytical prediction of the seismic behaviour of superelastic shape memory alloy reinforced concrete elements. *Engineering Structures*, Elsevier, **30**:3399-3411.

Alam, M.S., Youssef, M.A., and Nehdi, M. 2007. Utilizing shape memory alloys to enhance the performance and safety of civil infrastructure: a review. *Canadian Journal of Civil Engineering*, NRC Research Press, **34**(9):1075-1086.

Christopoulos, C., Filiatrault, A. and Folz, B. 2002. Seismic response of self-centring hysteretic SDOF systems. *Earthquake Engineering & Structural Dynamics*, Wiley, **31**(5):1131-1150.

Cortés-Puentes, W.L., and Palermo, D. 2015. Tension-Only SMA Bracing for Seismic Retrofitting. *The 5th International Conference on Construction Materials: Performance, Innovations and Structural Implications*, Whistler, BC, Canada.

Cortés-Puentes, W.L., Zaidi, M., Palermo, D. and Dragomirescu, E. 2018. Cyclic loading testing of repaired SMA and steel reinforced concrete shear walls. *Engineering Structures*, Elsevier, **168**:128-141.

Cruz-Noguez, C. and Saiidi, M. 2013. Performance of Advanced Materials during Earthquake Loading Tests of a Bridge System. *Journal of Structural Engineering*, ASCE, **1391**:144-154.

CSA. 2014. CSA-A23.3: Design of Concrete Structures. *Canadian Standard Association*, Mississauga, ON, Canada.

Elbahy, Y.I., Youssef, M.A. and Nehdi, M. 2009. Stress block parameters for concrete flexural members reinforced with superelastic shape memory alloys. *Materials and Structures*, **42**:1335-1351.

Eligehausen, R., Popov, E., and Bertero, V. 1983. *Local Bond Stress-Slip relationship of Deformed Bars under Generalized Excitations*. Earthquake Engineering Center, University of California, Berkeley, USA.

Ghassemieh, M., Rezapour, M. and Sadeghi, V. 2017. Effectiveness of the shape memory alloy reinforcement in concrete coupled shear walls. *Journal of Intelligent Material Systems and Structures*, SAGE, **285**:640-652.

Ghorbani-Renani, I., Velev, N., Tremblay, R., Palermo, D., Massicotte, B., I. and Léger, P. 2009. Modeling and Testing Influence of Scaling Effects on Inelastic Response of Shear Walls. *ACI Structural Journal*, ACI, **106**(3):358-367.

Kian, M.J.T. and Cruz-Noguez, C. 2018. Reinforced Concrete Shear Walls Detailed with Innovative Materials: Seismic Performance. *Journal of Composites for Construction*, **226**:04018052.

Luu, H., Ghorbani-Renani, I., Léger, P. and Tremblay, R. 2013. Numerical Modeling of Slender Reinforced Concrete Shear Wall Shaking Table Tests Under High-Frequency Ground Motions. *Journal of Earthquake Engineering*, Taylor & Francis, 17(4):517-542.

Maciel, M., Palermo, D., and Abdulridha, A. 2016. Seismic Response of SMA Reinforced Shear Walls. *Special Topics in Structural Dynamics*, Springer, 185-192.

Nehdi, M., Alam, M.S. and Youssef, M.A. 2011. Seismic behavior of repaired superelastic shape memory alloy reinforced concrete beam-column joint. *Smart Structures and Systems*, Techno-press, **7**:329-348.

NRC. 2015. Division B, Part4, Structural Design National Building Code of Canada. *National Research Council of Canada*, Ottawa, ON, Canada.

Park, R. 1988. Ductility Evaluation from Laboratory and Analytical Testing. *Ninth World Conference on Earthquake Engineering*, Tokyo-Kyoto, Japan, **VIII**:605-616.

Tarzav, M. and Saiidi M.S. 2015. Reinforcing NiTi Superelastic SMA for Concrete Structures. *Journal of Structural Engineering,* **141**:8.

Vecchio, F.J., Wong, P. and Trommels, H. 2013. *Vector2 and Formworks Manual*. 2nd ed. University of Toronto, Toronto, ON, Canada.

Youssef, M.A. and Elfeki, M.A. 2010. Seismic Performance of Shape Memory Alloy Reinforced Concrete Frames. *10th Canadian Conference on Earthquake Engineering*, Toronto, ON, Canada.